Nanothin Coculture Membranes with Tunable Pore Architecture and Thermoresponsive Functionality for Transfer-Printable Stem Cell-Derived Cardiac Sheets

Seungmi Ryu,[†,#] Jin Yoo,[‡,#] Yeongseon Jang,[‡] Jin Han,[§] Seung Jung Yu,[∥] Jooyeon Park,[§] Seon Yeop Jung,[⊥] Kyung Hyun Ahn,[§,⊥] Sung Gap Im,[∥] Kookheon Char,[*,‡] and Byung-Soo Kim[*,†,§,⊥]

[†]Interdisciplinary Program for Bioengineering, [‡]World Class University Program for Chemical Convergence for Energy and Environment, The National Creative Research Initiative Center for Intelligent Hybrids, [§]School of Chemical and Biological Engineering, and [⊥]Institute of Chemical Process, Seoul National University, Seoul 151-744, Republic of Korea and [∥]Department of Chemical and Biomolecular Engineering & KI for Nano Century, Korea Advanced Institute of Science and Technology, Daejeon 305-701, Republic of Korea. [#]These authors contributed equally.

ABSTRACT Coculturing stem cells with the desired cell type is an effective method to promote the differentiation of stem cells. The features of the membrane used for coculturing are crucial to achieving the best outcome. Not only should the membrane act as a physical barrier that prevents the mixing of the cocultured cell populations, but it should also allow effective interactions between the cells. Unfortunately, conventional membranes used for coculture do not sufficiently meet these requirements. In addition, cell harvesting using proteolytic enzymes following coculture impairs cell viability and the extracellular matrix (ECM) produced by the cultured cells. To overcome these limitations, we developed nanothin and highly porous (NTHP) membranes, which are ~20-fold thinner and ~25-fold more porous than the conventional coculture membranes. The tunable pore size of NTHP membranes at the nanoscale level was found crucial for the formation of direct gap junctions-mediated contacts between the cocultured cells. Differentiation of the cocultured stem cells was dramatically enhanced with the pore size-customized NTHP membrane system compared to conventional coculture methods. This was likely due to effective physical contacts between the cocultured cells and the fast diffusion of bioactive molecules across the membrane. Also, the thermoresponsive functionality of the NTHP membranes enabled the efficient generation of homogeneous, ECM-preserved, highly viable, and transfer-printable sheets of cardiomyogenically differentiated cells. The coculture platform developed in this study would be effective for producing various types of therapeutic multilayered cell sheets that can be differentiated from stem cells.

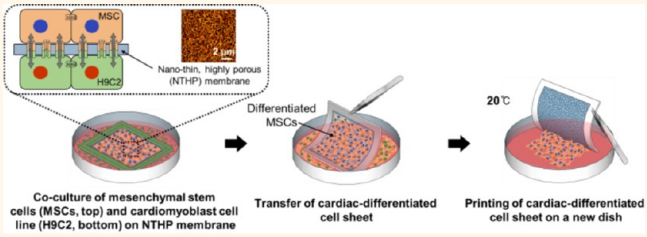

KEYWORDS: cardiac differentiation · coculture · membrane · mesenchymal stem cells · transfer-printing

Stem cell therapy has been spotlighted as a promising approach for various types of disease treatments and tissue regeneration. However, despite their multipotency, transplantations of naïve stem cells have shown low differentiation efficiency *in vivo*.[1] Such outcomes are the result of the incompatible physicochemical characteristics of stem cells with the surrounding *in vivo* environment,[1,2] discouraging the creation of an optimal milieu for tissue repair. Thus, inducing stem cell differentiation into the desirable cell type, prior to implantation, has been proposed to improve their therapeutic results.[1−3] The differentiation of stem cells can be regulated by the surrounding microenvironment, the so-called stem cell niche.[4] Several approaches, such as introducing bioactive molecules or scaffolds that provide the biomimetic microenvironments, have been reported to promote the differentiation of stem cells.[5−7] However, such artificial microenvironments may be insufficient in mimicking the complex nature of native microenvironments to regulate the differentiation

* Address correspondence to khchar@plaza.snu.ac.kr, byungskim@snu.ac.kr.

Received for review June 23, 2015 and accepted September 11, 2015.

Published online September 11, 2015
10.1021/acsnano.5b03823

of stem cells.[8] Instead, coculturing stem cells with the desired type of differentiated cells is highly effective in controlling their fate.[9−11] The coculture strategy induces stem cell differentiation by providing the naturally occurring cell-to-cell cross-talk, either through soluble paracrine factors or direct cell−cell contact, mimicking the native tissue microenvironment.[12] In addition, the coculture strategy is often more cost-effective than dosing the culture medium with specific biomolecules, including growth factors.[13] Several studies using coculture have reported effective stem cell differentiation into osteoblast,[9] cardiomyocyte,[10] neuronal, and glial cells.[11]

The features of the membrane used in coculture systems are critical to stem cell differentiation outcomes. The membrane should allow effective cell-to-cell cross-talk between the heterogeneous cells (i.e., stem cells and the desired type of differentiated cells), while at the same time serve as a physical barrier to prevent mixing of the cells for efficient cell separation following coculture.[14,15] "Transwell" is a commercially available porous membrane that is conventionally used for coculture. However, because of the "track-etched" fabrication method, a Transwell membrane is more than 10 μm thick and has a low porosity.[14] A previous study demonstrated that the physical properties of Transwell membranes hinder sufficient physical contact between cocultured heterogeneous cells and the diffusion of bioactive molecules, secreted by the cultured cells across the membrane.[16] Thus, developing an ultrathin, highly porous membrane that allows effective direct cocultured cellular contacts and paracrine factor diffusion across the membrane is required for efficient stem cell differentiation.

In addition, enzymatic harvesting of cells following coculture is a major drawback of conventional coculture systems, since such methods damage the extracellular matrices (ECM) produced by the cultured cells and reduce their viability. This results in poor survival and low therapeutic efficacy of the implanted cells.[17,18] This poor survival also hampers the functional benefits of the cell therapy.[19] As an approach that can overcome such problem, cell sheet engineering has attracted considerable interest. The preservation of ECM of the cell sheet was reported to facilitate cell survival and engraftment after implantation.[18,20] Moreover, implanting multilayered cell sheets was reported to result in better therapeutic outcomes than single-layered cell sheets, as more cell−cell junctions and ECM resulted in better reparative effects of the cells.[21−23]

Here, we report the development of nanothin and highly porous (NTHP) membranes with a thermoresponsive property for generating transfer-printable sheets of cells differentiated from stem cells through coculture. The nanothin and highly nanoporous architecture of the NHTP membrane was realized by a vapor-induced phase separation (VIPS) mechanism using a spin-coating process. By using this process, the pore size of NTHP membranes was finely tuned at the nanoscale level by changing the process parameters and conditions. The NTHP membranes are ~20-fold thinner and ~25-fold more porous than conventional "Transwell" membranes. Also, the initiated chemical vapor deposition (iCVD) process was employed to graft a thermoresponsive layer conformally onto the NTHP membranes without altering their porous structure. We hypothesized that such features of the NTHP membrane would induce effective differentiation of stem cells into the desired cell type through coculture. The NTHP membrane would allow active cell-to-cell communication between the heterogeneous cocultured cells, as it significantly shortens the distance between the cells to the nanoscale level, creating a more *in vivo*-like environment. At the same time, the NTHP membrane would function as an effective physical barrier preventing cell cross-contamination. Another expected benefit of the free-standing, thermoresponsive NTHP membrane is that it can generate a transfer-printable cell sheet in response to temperature change. The NTHP membrane would allow easy harvesting of the differentiated cell sheets after coculture due to its free-standing, transferable property. In addition, it could be used to print the differentiated cell sheets to form multilayered cell sheets or tissue for implantation. The ECM of the cell sheets are preserved with this technique, which would enhance the therapeutic efficacy of the cells following implantation. In short, the NTHP membrane developed in this study can be used as an effective coculture tool for engineering multilayered sheets of differentiated cells originating from stem cells, and serve as a promising modality for cell therapy.

RESULTS AND DISCUSSION

Fabrication and Characterization of NTHP Membrane. Figure 1A illustrates the procedure for the fabrication of the thermoresponsive NTHP membrane. When a nonsolvent in the liquid phase comes in contact with a polymer solution, mass exchange between the polymer solution and nonsolvent occurs rapidly, forming macrovoids in the membrane.[24] To induce the nanoscale pore architecture, the mass exchange rate was slowed by using the vapor phase of the nonsolvent (i.e., water), with controlled relative humidity (RH), during the spin-coating process. RH has a decisive effect on the number and size of pores as it results in different composition paths as shown in the ternary phase diagram (Figure 1B).[25] Among the various process parameters in designing VIPS-based membranes,[26] in this study, the pore size of the NTHP membrane was tuned by controlling the RH, spin-rate, and different types of solvent in polymer solution. NTHP membranes with distinctively different sizes of well-defined pores (i.e., an average of 100, 380,

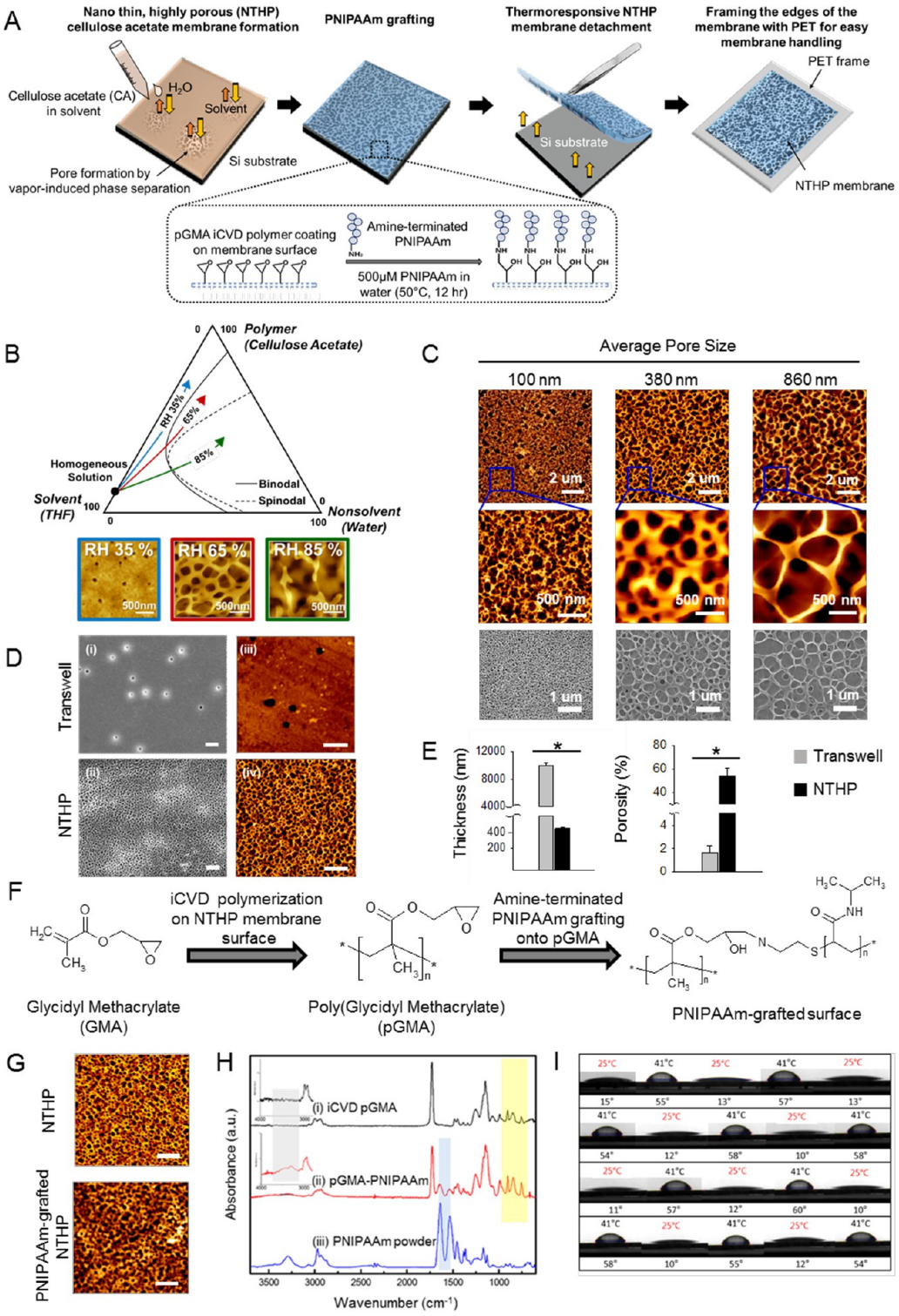

Figure 1. Fabrication and characterization of NTHP membranes with tunable pore architecture used in this study. (A) A schematic diagram showing the fabrication of thermoresponsive NTHP membranes. (B) VIPS composition paths of NTHP membranes in a ternary phase diagram and the corresponding AFM images obtained at different RH. Bars, 500 nm. (C) Morphologies of NTHP membranes with different pore sizes. (D) SEM and AFM images of (i, ii) a Transwell membrane and (iii, iv) an NTHP membrane. Bars, 2 μm. (E) Thickness and porosity of a Transwell membrane and an NTHP membrane (with comparable pore size of 400 and 380 nm, respectively). *$p < 0.05$. (F) Schematic of the chemical reactions for the iCVD polymerization of GMA monomers and the grafting of PNIPAAm onto the pGMA-coated NTHP surface. (G) AFM images of NTHP membranes before and after the grafting of PNIPAAm. Bars, 2 μm. (H) FT-IR spectra of (i) iCVD pGMA polymer, (ii) PNIPAAm-grafted surface, and (iii) PNIPAAm powder. (I) Water contact angle measurements of the PNIPAAm-grafted surfaces at different temperatures.

and 860 nm pore size, respectively, with similar thickness) can be generated by changing the process parameters (Figure 1C, Supporting Information, Figure S1, and Table S1).

The surface morphologies of commercial Transwell and our NTHP membranes (with comparable pore size of 400 and 380 nm, respectively) were examined and compared by scanning electron microscopy (SEM) and atomic force microscopy (AFM) (Figure 1D). While the thickness and porosity of the Transwell membrane were 10 μm and 2%, respectively, those of the NTHP membrane were 380 nm and 54%, respectively (Figure 1E). This highlights the nanothin and highly porous architecture of the developed NTHP membrane.

To harvest transfer-printable cell sheets from NTHP membranes, the surface of the membrane was grafted with a thermoresponsive polymer, poly(*N*-isopropylacrylamide) (PNIPAAm).[27] Previous studies reported that changes in hydration of PNIPAAm polymer in response to temperature can alter the cellular adhesiveness/nonadhesiveness of the PNIPAAm-grafted surface.[27−30] Above the lower critical solution temperature (LCST) in an aqueous solution of 32 °C, PNIPAAm-grafted polymer become mildly hydrophobic since the conformation of the PNIPAAm polymer chains collapses. The collapsed state of PNIPAAm polymer chains promotes adsorption of cell-adhesive proteins (e.g., fibronectin) on the PNIPAAm-surface and allows subsequent cellular adhesion. Below the LCST, the PNIPAAm-grafted polymer rapidly swells and becomes highly hydrophilic. The entropic repulsion of the protein adsorption initiates the detachment of the cells.[31] To conformally graft a PNIPAAm layer onto NTHP membranes, while preserving the porous structure of the membranes, the iCVD method was adopted. iCVD is an effective method of coating various types of functional polymer thin films uniformly onto complex surfaces, including nanopatterned substrates and nanoporous membranes without altering the substrate structure and properties.[32] The NTHP membranes were initially coated with an epoxy-containing linker layer composed of poly(glycidyl methacrylate) (pGMA),[33] followed by a grafting reaction with amine-terminated PNIPAAm using an epoxy-amine addition reaction (Figure 1F). This method successfully preserved the highly porous architecture of the NTHP membrane even after PNIPAAm engraftment (Figure 1G).

The chemical compositions of deposited polymer films were examined by Fourier transform infrared spectroscopy (FT-IR) (Figure 1H and Figure S2) and X-ray photoelectron spectroscopy (XPS) (Supporting Information Figure S3 and Table S2). In the FT-IR spectrum of the pGMA-coated membrane, the characteristic epoxy pendant peaks at 760, 847, and 908 cm^{-1} were clearly identified (yellow box in Figure 1H), indicating that the GMA monomers were successfully polymerized by the iCVD process without degradation of the epoxy functionality of the GMA monomer. This result was fully consistent with our previous study (Figure S2).[34] The FT-IR spectrum of the PNIPAAm-immobilized surface clearly showed the increase of the secondary amides N−H stretching vibrations (3370−3270 cm^{-1}), compared to the pristine pGMA deposited surfaces, confirming the PNIPAAm functionalization onto the NTHP membranes (gray box of inset spectra). Furthermore, in comparison with PNIPAAm powder, the decreased primary amine peak intensity of the PNIPAAm-immobilized surface clearly illustrated that the primary amine functionality in the amine-terminated PNIPAAm was consumed by the epoxy-amine addition reaction with the surface pGMA linker layer (blue box). A sharp, reversible phase transition of the PNIPAAm-grafted surface was monitored by measuring the water contact angle change with repeated temperature variation (Figure 1I), demonstrating the thermoresponsive property of the PNIPAAm-grafted NTHP membranes.

Biocompatibility of NTHP Membrane as Cell Culture Substrate. To investigate the biocompatibility of the NTHP membrane, human bone-marrow derived mesenchymal stem cells (MSCs) were cultured on tissue culture polystyrene (TCPS) dishes, Transwell membranes (Transwell), and NTHP membranes (NTHP). The viability, apoptotic activity, and proliferative activity of MSCs on each surface were measured for comparison. The numbers of live cells were obtained at various time points using a Cell Counting Kit-8 assay. The assay revealed no significant differences in the number of live cells among the groups (Figure 2A). In addition, we examined the expressions of a pro-apoptotic regulatory gene, BAX, and an antiapoptotic regulatory gene, Bcl-2, on day 3 of the MSC culture. The data showed that MSCs on TCPS, Transwell, and NTHP membranes expressed comparable levels of apoptosis-regulatory genes (Figure 2B). Proliferating cell nuclear antigen (PCNA) staining on day 3 and day 7 also indicated comparable proliferation of MSCs between the groups (Figure 2C). Collectively, the data indicate that the NTHP membrane is a biocompatible cell culture substrate.

Coculture Using Thermoresponsive NTHP Membrane for the Generation of Transfer-Printable Cell Sheet. Scheme 1 illustrates the NTHP-based coculture system for generating transfer-printable differentiated cell sheets originating from cocultured stem cells. MSCs were seeded on the PNIPAAm-grafted surface of NTHP membranes at 37 °C. H9C2 cells (H9C2s), a cardiomyoblast cell line, were seeded on culture dishes. Following this, the MSC-seeded NTHP membrane was layered on top of the H9C2-seeded culture dish for coculture. To secure the membrane stacking on H9C2s and prevent membrane displacement during coculture, a square stainless steel ring was placed on top of the membrane. MSCs were cocultured with H9C2s to induce the

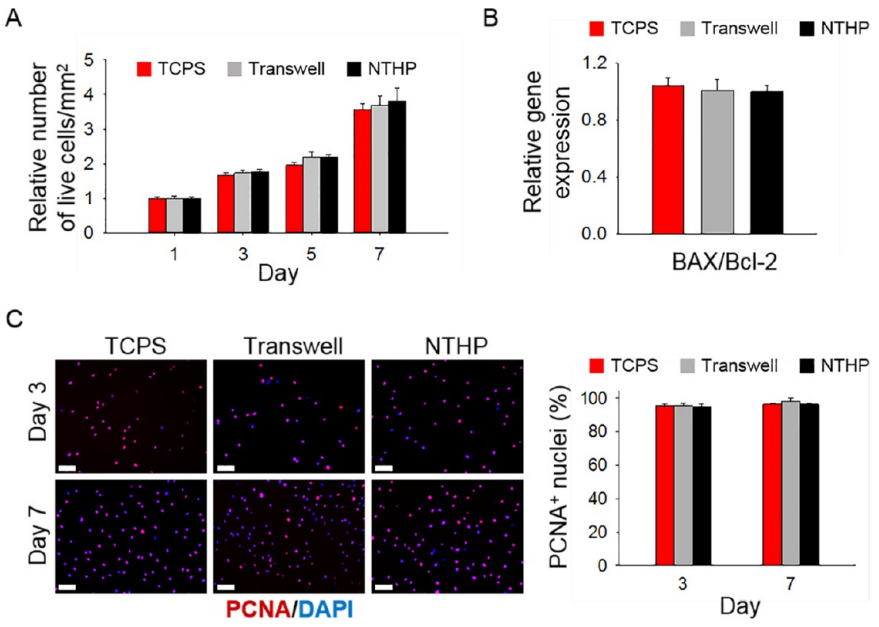

Figure 2. Biocompatibility of NTHP membranes evaluated in terms of live cell number, proliferation, and apoptotic activity of MSCs cultured on the membranes. (A) The number of live cells expressed relative to the number of live cells on tissue culture polystyrene (TCPS) dish at day 1. The data were obtained using the CCK-8 assay. (B) Changes in expressions of apoptosis regulatory genes, a pro-apoptotic marker BAX and an antiapoptotic marker Bcl-2, in MSCs cultured on various surfaces for 3 days evaluated by qRT-PCR. (C) Images and quantification of proliferating cells evaluated by PCNA immunocytostaining. PCNA$^+$ (red) cells are proliferating cells. DAPI (blue) stains nuclei. Bars, 100 μm.

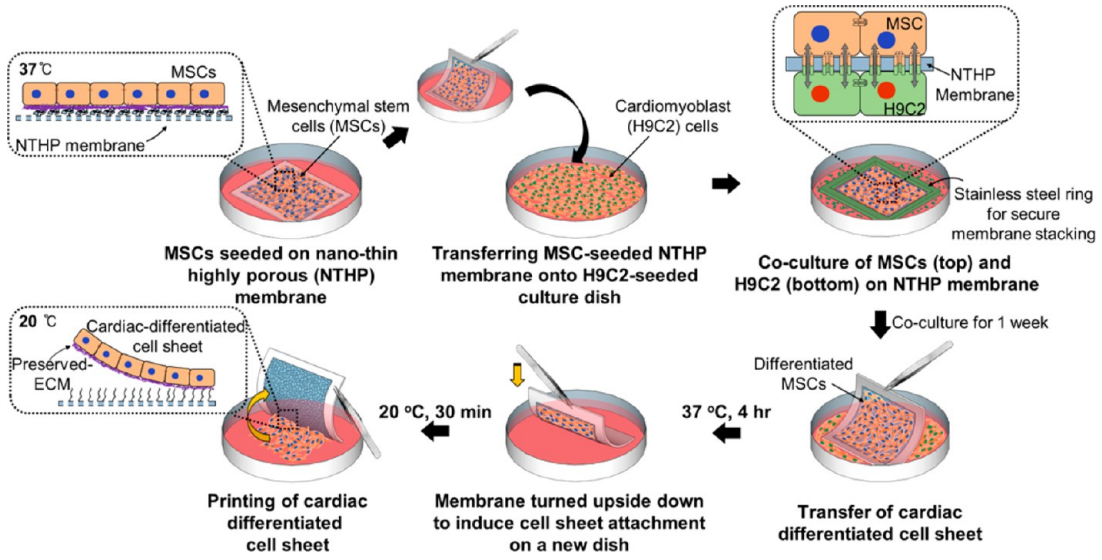

Scheme 1. Schematic illustrations of the NTHP membrane-based generation of transfer-printable sheets of differentiated cells through co-culture.

cardiac differentiation of MSCs by simulating the niche of MSCs with paracrine factors secreted from H9C2s and direct MSCs-H9C2s contact across the NTHP membrane.[35] After 1 week of coculture, the NTHP membrane, originally seeded with MSCs, was transferred from the H9C2-cultured dish onto a new culture dish. At a lower temperature of 20 °C, a sheet of cardiac-differentiated cells was printed on to the new dish.

Varying Extents of Cellular Interactions between Cocultured Cells Depending on the Different Pore Sizes of NTHP Membranes. To determine the ideal pore size of NTHP membranes that would support maximum cell-to-cell communication (*i.e.*, diffusion of paracrine soluble factors and cell junctions-mediated direct contacts), the extents of cellular interactions between the cocultured MSCs and H9C2s were examined. Cellular proximity along with protein diffusion across the NTHP membranes with varying pore sizes were evaluated and compared to Transwell membranes. We also analyzed whether the pore dimensions of the membranes affect the

functional gap-junction-mediated direct cell-to-cell cross-talk between MSCs and H9C2s using the calcein-AM dye transfer assay.

To observe the cell-to-cell proximity between MSCs and H9C2s, each cell type was labeled with different colored dyes: MSCs with green and H9C2s with red (Figure 3A). The side view of the cocultured MSCs and H9C2s, separated by a Transwell membrane, showed that the distance between the cocultured cells was as far as 10 μm, which corresponds to the thickness of the Transwell membrane (Figure 3Aii). In contrast, the cocultured MSCs and H9C2s in the NTHP membrane systems were in close contact (Figure 3A iv, vi, and viii). However, the distances between the cells using NTHP membranes with 380 and 860 nm pore sizes (NTHP-380 and NTHP-860, respectively) were in closer proximity (within the 200 nm resolution of super-resolution confocal microscopy) compared to cells cultured on 100 nm pore size membrane (NTHP-100), as some parts of the cells were observed in yellow due to the colocalized pixels of green and red fluorescence (arrows in Figure 3A v and vii).

Next, to compare the rate of protein diffusion through the NTHP membrane versus the Transwell membrane, mathematical modeling and empirical studies on protein diffusion were conducted. To evaluate the effects of thickness and porosity of the membrane on the interphase transfer of protein molecules, we employed a simplified one-dimensional mathematical model that was established in a previous study.[36]

$$\frac{\partial C}{\partial t} = D_{\text{eff}}\frac{\partial^2 C}{\partial x^2} \quad (D_{\text{eff}} = D_0 f(C_0, C_s)h[\varepsilon, \zeta, L(X)]) \qquad \text{(A)}$$

where C is the concentration of proteins, D_0 the diffusion coefficient in water, D_{eff} the effective diffusion coefficient of proteins which is influenced by the physical properties of the solute, $f(C_0, C_s)$, and the microstructural properties of the membrane, $h[\varepsilon, \zeta, L(X)]$. In addition, a hindrance factor of the diffusion coefficient,[37] which accounts for the decrease in the rate of diffusion in less porous material, was proposed as

$$\frac{D_{\text{eff}}}{D_0} \cong \frac{2\theta}{3-\theta} \qquad \text{(B)}$$

eq A combined with eq B was solved numerically under proper boundary conditions. The results indicated that protein diffusion occurred faster when the membrane thickness is reduced (Figure S4) and the membrane porosity is increased (Figure S5).

Subsequently, a chamber was designed to empirically compare the rate of protein diffusion through the NTHP and Transwell membranes. Each membrane was set to partition the protein diffusion chamber into two secluded compartments. One compartment was filled with 10 mL of 10 μg/mL bovine serum albumin (BSA) solution, while the other was filled with phosphate buffer saline (PBS) of equal volume. Thus, BSA was allowed to diffuse into the PBS chamber only through the separating porous membrane (Figure 3B). The result showed that the BSA diffusion rate was not affected by the pore sizes of NTHP membranes (Figure 3Bi), which was likely due to the comparable porosity and thickness among the membranes (Table S1). However, the BSA diffusion rate was significantly higher in the NTHP membrane system compared to the Transwell membrane system (Figure 3Bii), which can be attributed to the reduced thickness and higher porosity of the NTHP membranes (Figure 1E).[36,37]

To investigate whether the cocultured MSCs and H9C2s were undergoing active direct cell-to-cell cross-talk *via* gap junctions, a calcein-AM dye transfer assay was performed (Figure 3C). MSCs, on the top side of each membrane, were dual-labeled with DiI (red) and calcein-AM (green). DiI is a dye that labels cell membranes and cannot be transferred through direct cell−cell contact. Calcein-AM is nonfluorescent outside cells. However, once calcein-AM penetrates cells, it is cleaved to fluorescent calcein by esterase within the cells.[38] The fluorescent calcein is cell membrane-impermeant and can pass only through direct cell-to-cell gap junction channels.[39] Thus, without direct cell-to-cell connections, calcein cannot diffuse from MSCs into the underlying H9C2s during the dye transfer assay. The results showed that calcein-AM was not transferred to H9C2s (green color only) in the Transwell system (Figure 3Ci). The side view of the cocultured cells clearly showed that none of the H9C2s (arrow heads in Figure 3Cii) on the bottom side of the Transwell membrane (indicated by yellow dashed line) exhibited green fluorescence, indicating that there was no calcein-AM transfer across the Transwell membrane (Figure 3Cii). This is due to the large thickness and low porosity of the Transwell membrane, which fails to permit effective cell−cell contact between the cocultured MSCs and H9C2s layers. In addition, calcein-AM was not transferred to H9C2s across the NTHP-100 membrane system (arrowheads in Figure 3Civ), indicating that despite close proximity the cells were not forming direct cell−cell contacts. In contrast, calcein-AM transferred H9C2s were observed in the NTHP-380 and NTHP-860 systems. (Figure 3Cv and Figure 3Cvii). The side view also revealed extensive calcein-AM transfer across the NTHP membrane from the top MSC layer to the bottom H9C2s layer (arrows in Figure 3Cvi and viii). These data clearly indicate that while the ultrathin thickness and high porosity of the NTHP membrane allows dynamic and direct MSCs-H9C2s contact *via* gap junctions, the nanoscale pore sizes of the membranes also play a crucial role in the formation of gap junctions between the cocultured cells. Finally, we found that NTHP membranes with pore size below 100 nm were not ideal for direct

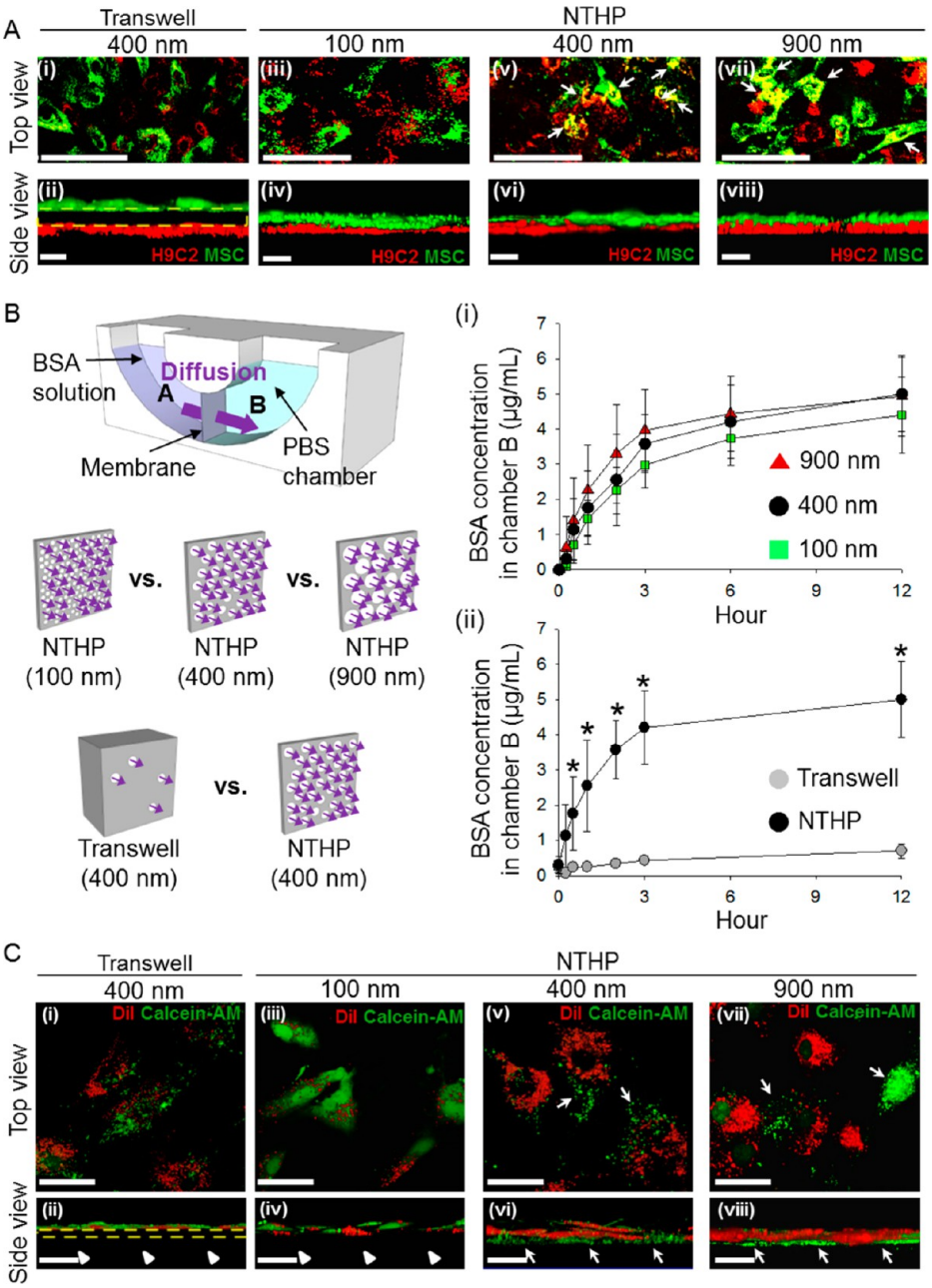

Figure 3. Assessments of direct intercellular interactions in the coculture systems and the rates of protein diffusion through the membranes. (A) Confocal images of cocultured MSCs (green) and H9C2s (red) viewed from the (i, iii, v, and vii) top (bars, 100 μm) and (ii, iv, vi, and viii) side (bars, 20 μm). The Transwell membrane is marked with yellow dashed lines. MSCs and H9C2s in close proximity (within the 200 nm resolution of super-resolution confocal microscopy) were yellow due to the colocalized pixels of green and red fluorescence (arrows in v and vii). (B) Illustration of protein diffusion chamber experiment and quantitative analysis of the rate of BSA molecule diffusion through NTHP membranes depending on (i) various sizes of the nanopores of the membranes and (ii) compared to Transwell membranes. *$p < 0.05$. (C) Confocal images of calcein-AM (green) dye transfer between cocultured MSCs and H9C2s *via* gap junctions. Prior to coculture, MSCs were dual-labeled with DiI (red) and calcein-AM (green). Only cells that form direct contact would show calcein−AM (green) transfer from MSCs (on top of the membrane) to H9C2s (on bottom of the membrane). Confocal images of the (i and iii) top and (ii and iv) side views of Transwell and NTHP membranes with a pore size of 100 nm show dual-labeled MSCs (red and green) on the top of the membrane with no calcein-AM (green) transfer to the H9C2s (no green, arrow heads in (ii) and (iv)) on the bottom of membrane, showing the absence of direct contact between the cells in both systems. The Transwell membrane is marked with yellow dashed lines. In contrast, confocal images of the (v and vii) top and (vi and viii) side views of NTHP membranes with pore sizes of 380 and 860 nm, respectively, indicate calcein-AM (green) transfer from dual-labeled MSCs (red and green) on the top of NTHP membrane to H9C2s (green only, arrows in (vi) and (viii)) on the bottom, demonstrating direct contact between MSCs and H9C2s. Bars, 50 μm.

cell−cell gap junction-mediated interactions between the cocultured cells.

Facile, Homogeneous Collection of MSCs Postculture. For cardiac differentiation of stem cells through coculture,

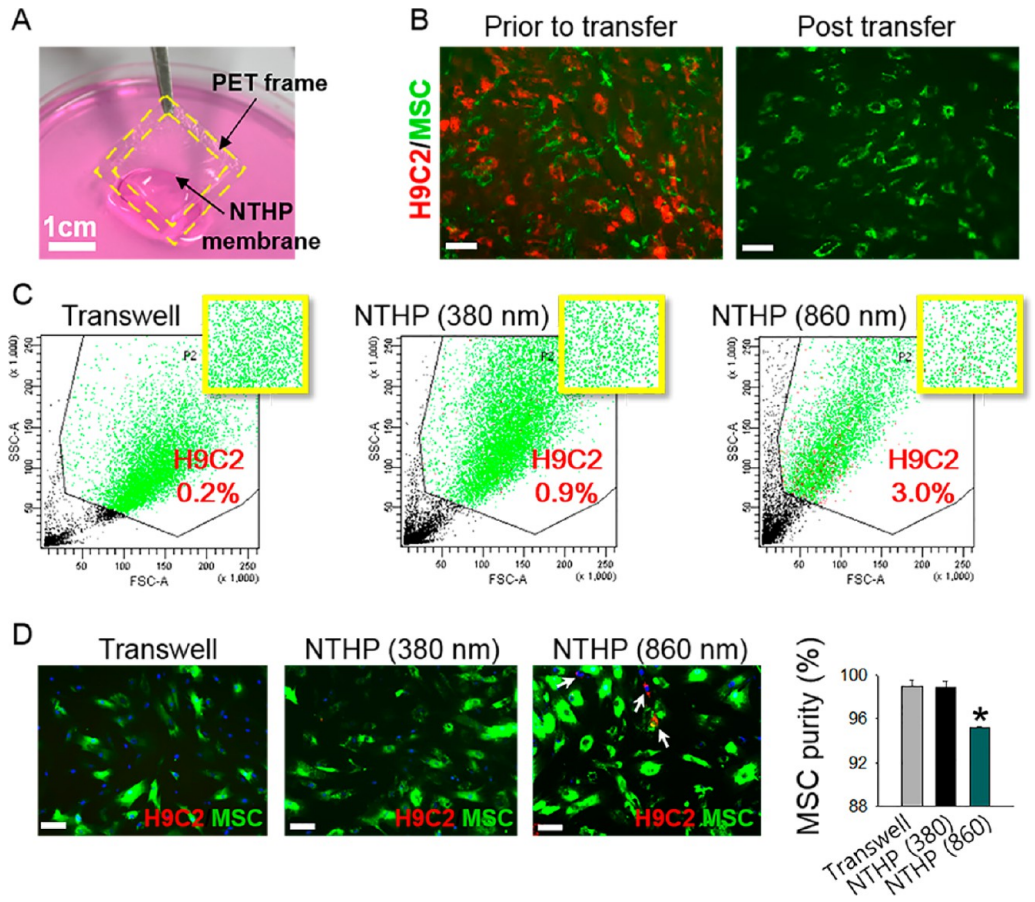

Figure 4. Facile collection of MSCs and assessing their purity following coculture with H9C2s, using the transferable NTHP membrane. (A) Photograph showing the transfer of MSCs cultured on PET-framed NTHP membrane following coculture with H9C2s. The PET frame is marked using yellow dashed lines. (B) Fluorescent images of MSCs (green) and H9C2s (red) cocultured on the top and bottom sides of the NTHP membrane and the MSCs collected following transfer of the NTHP membrane (pore size of 380 nm) onto a new dish. Bars, 100 μm. (C) Homogeneity of the collected MSCs analyzed by FACS analysis. MSCs are expressed in green and H9C2s in red. (D) Fluorescent images and quantification of the MSCs collected and replated on a new culture dish to analyze their purity. Bars, 100 μm. *$p < 0.05$ vs other groups.

the use of allogeneic cardiac cells or cell lines is inevitable due to limited access to human primary cardiac cells.[40] For therapeutic applications, the homogeneity of the collected cells postcoculture should be strictly preserved as contamination of the collected cells with exogenous cells might result in serious complications such as immune rejection after *in vivo* transplantation.[41] Thus, the role of the membrane as a physical barrier between the two types of cell populations is important to prevent the cross contamination and preserve the homogeneity of the cells.

A remarkable feature of the NTHP membrane system is facile harvesting of MSCs from the cocultured cell populations. Owing to its free-standing capability, the NTHP membrane is readily transferable, facilitating the fast and easy collection of cultured MSCs (Figure 4A). Green fluorescence dye (DiO)-labeled MSCs, which have been cocultured with red fluorescence dye (DiI)-labeled H9C2s, were exclusively isolated from the cocultured cell populations by NTHP membrane transfer after 1 week of coculture, demonstrating the fast and simple harvesting of MSCs with NTHP membranes (Figure 4B).

To determine whether NTHP membranes effectively prevent cellular cross-contamination across the membranes, the homogeneity of the collected MSCs after 1 week of coculture was assessed using fluorescence-activated cell sorting (FACS) (Figure 4C) and fluorescence microscopy (Figure 4D). The quantitative analysis by FACS and qualitative observation through fluorescence microscopy revealed that the homogeneity of the collected MSCs from the NTHP-380 membrane was high and comparable to that from commercial Transwell membrane. This demonstrated the robust function of the NTHP-380 membrane as a competent physical barrier between the cocultured cells. In addition, the data indicated that adhesion of H9C2s on to the culture dish was strong enough to prevent their detachment upon transfer of the NTHP membrane, contributing to the high purity of the collected MSCs (Figure 4D). However, the impurity of the collected MSCs from the NTHP-860 membrane system was much higher compared to to that of both MSCs collected from Transwell and NTHP-380 systems (Figure 4C and Figure 4D). These data were consistent

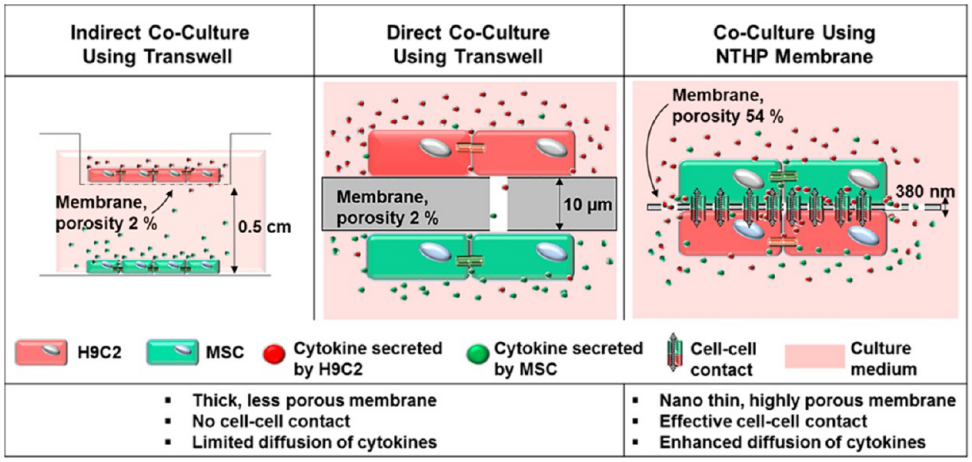

Scheme 2. Comparison of the NTHP Membrane-Based Coculture System with the Conventional Transwell Coculture Systems

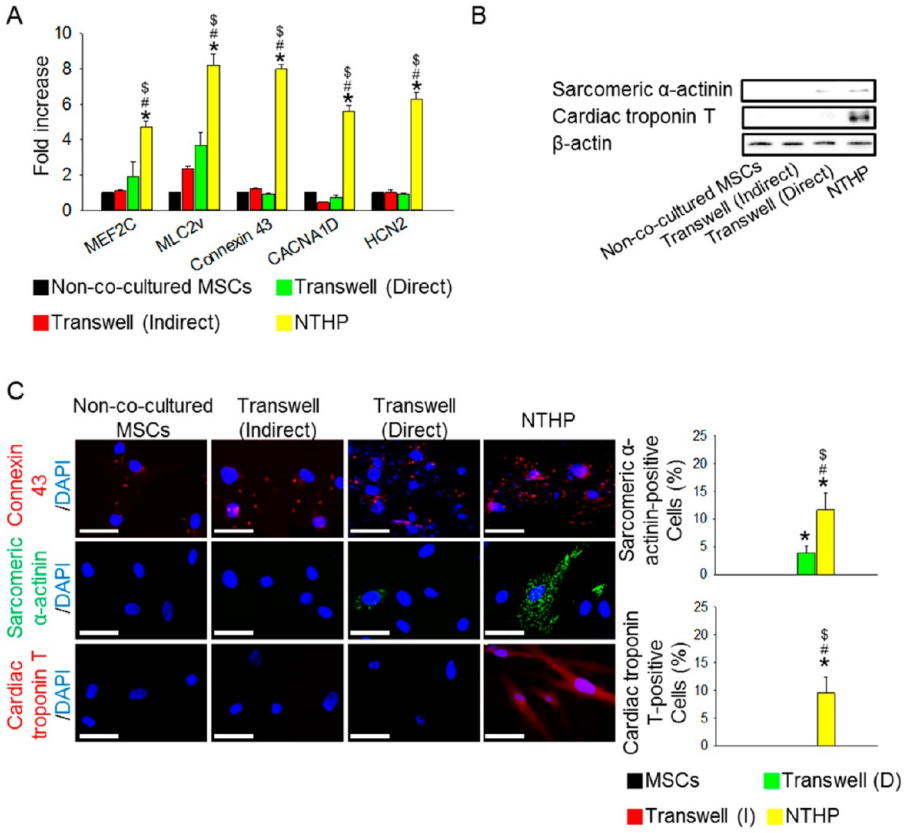

Figure 5. Enhanced cardiac differentiation of MSCs in the NTHP membrane system following 1 week of coculture with H9C2s. (A) mRNA expression levels of cardiac transcription factor (MEF2C), cardiac structural marker (MLC2v), gap junction marker (connexin 43), and cardiac ion channel markers (CACNA1D, HCN2) in MSCs after coculture. Gene expression levels were normalized to those of noncocultured MSCs. (B) Western blot analysis for cardiac structural proteins, sarcomeric α-actinin, and cardiac troponin T of MSCs after coculture. (C) Immunocytochemistry of cardiac protein markers and quantification for the cardiac specific marker-positive MSCs after coculture. Bars, 50 μm. *$p < 0.05$ *vs* noncocultured MSCs. $^{\#}p < 0.05$ *vs* Transwell (indirect). $^{\$}p < 0.05$ versus Transwell (direct).

with a previous study that indicated cellular cross-migrations in cocultured populations separated by membranes with pore sizes around 1 μm.[42] Collectively, we deduced that the ideal pore size for the NTHP membrane system that allows dynamic interactions between the cocultured cells and at the same time acts as a robust physical barrier between them is 380 nm.

Enhanced Differentiation of MSCs by NTHP Coculture System. Previous studies have reported that naïve MSC transplantation for myocardial infarction treatment is insufficient to achieve the best therapeutic outcome because transplanted MSCs rarely differentiate into cardiomyocytes *in vivo*, and the physiological characteristics of naïve MSCs is inharmonious with the heart

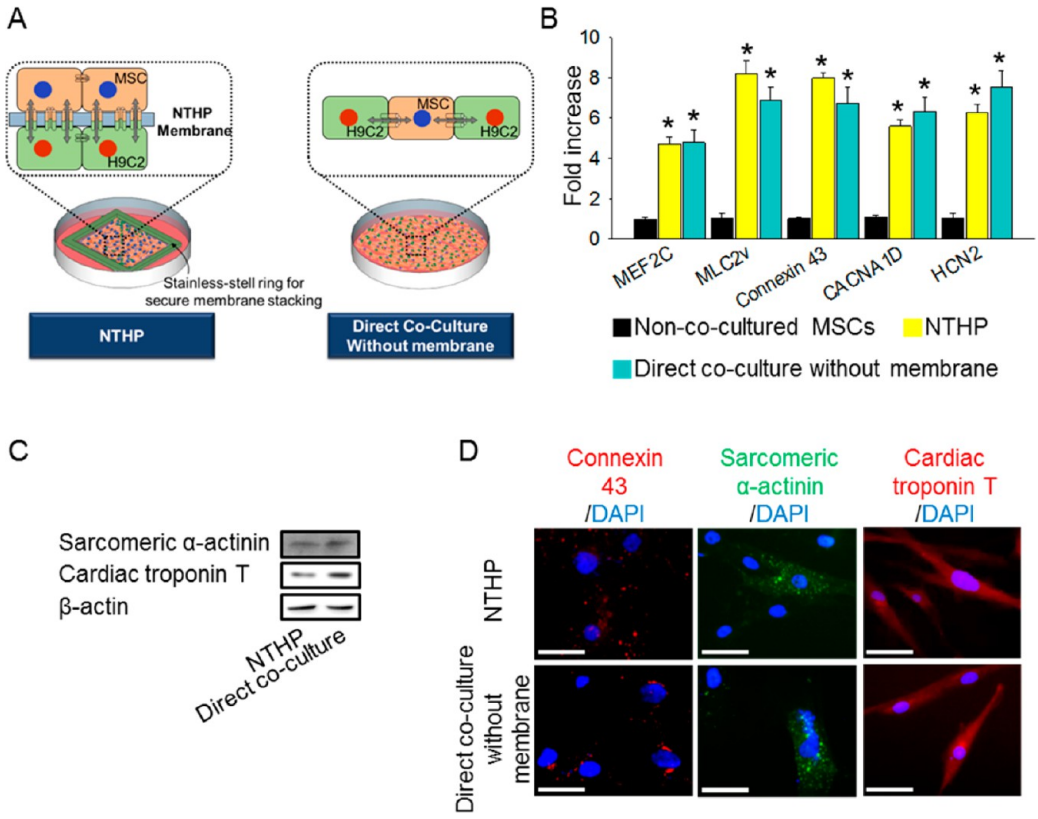

Figure 6. Comparison of cardiac differentiation of MSCs in the NTHP membrane coculture system and in the direct coculture system without membrane. (A) Schematic illustrations of NTHP membrane-based coculture and direct coculture without membrane. (B) mRNA expression levels of cardiac transcription factor (MEF2C), cardiac structural marker (MLC2v), gap junction marker (connexin 43), and cardiac ion channel markers (CACNA1D, HCN2) in MSCs after coculture for 1 week. Gene expression levels were normalized to the levels of noncocultured MSCs. *$p < 0.05$ versus noncocultured MSCs. No significant differences between NTHP and direct coculture were observed. (C) Western blot analyses for cardiac structural proteins, sarcomeric α-actinin and cardiac troponin T of MSCs after coculture for 1 week. (D) Immunocytochemistry for cardiac protein markers of MSCs after coculture for 1 week. Bars, 50 μm.

tissue, imposing the risk of arrhythmia.[3,43−45] The transplantation of MSCs that express cardiac biomarkers was reported to have better reparative effects.[46,47] Thus, cardiac differentiation of MSCs *ex vivo* prior to transplantation is a high-priority requirement for improved therapeutic efficacy of MSCs for cardiac repair. As coculturing with cardiomyoblasts was shown to promote cardiac-lineage differentiation,[48] we investigated whether the cardiac differentiation of MSCs could be achieved through coculture with H9C2s on NTHP membranes. Scheme 2 briefly illustrates the advantages of the NTHP membrane system as a new coculture system over the conventional "Transwell" system. In general, there are two coculture methods in the "Transwell" system: indirect coculture and direct coculture. In the indirect coculture method, H9C2s, which provide important cues for the cardiac differentiation of MSCs, are seeded on the porous membrane of the Transwell insert, while the MSCs are seeded on the bottom chamber. This coculture system induces stem cell differentiation only *via* indirect intercellular communication, which is the diffusion of cytokines secreted by H9C2s across the porous membrane. Direct cell−cell contact is absent in this system. The other method is the direct coculture method, in which H9C2s are seeded on the porous membrane of the Transwell insert and MSCs are seeded on the opposite side of the porous membrane. This system is expected to allow both the diffusion of cytokines secreted by H9C2s and direct cell−cell contact through the microthin, porous Transwell membrane. In contrast, our NTHP membrane system benefits from a nanothin, highly porous membrane, which enables dynamic crosstalk between H9C2s and MSCs through faster cytokine diffusion and more effective cell−cell contact compared to the Transwell system.

The expressions of cardiac-associated genes and proteins were assessed after 1 week of culturing MSCs in various conditions: noncocultured, cocultured with H9C2s using the Transwell indirect coculture system (Transwell (Indirect)), cocultured with H9C2s using the Transwell direct coculture system (Transwell (Direct)), and cocultured with H9C2s using the NTHP coculture system (NTHP). Gene expressions of a cardiac transcription factor (MEF2C), a cardiac structural marker (MLC2v), a gap junction marker (connexin 43), and cardiac ion channel markers (CACNA1D, HCN2) were significantly higher in the NTHP group (Figure 5A).

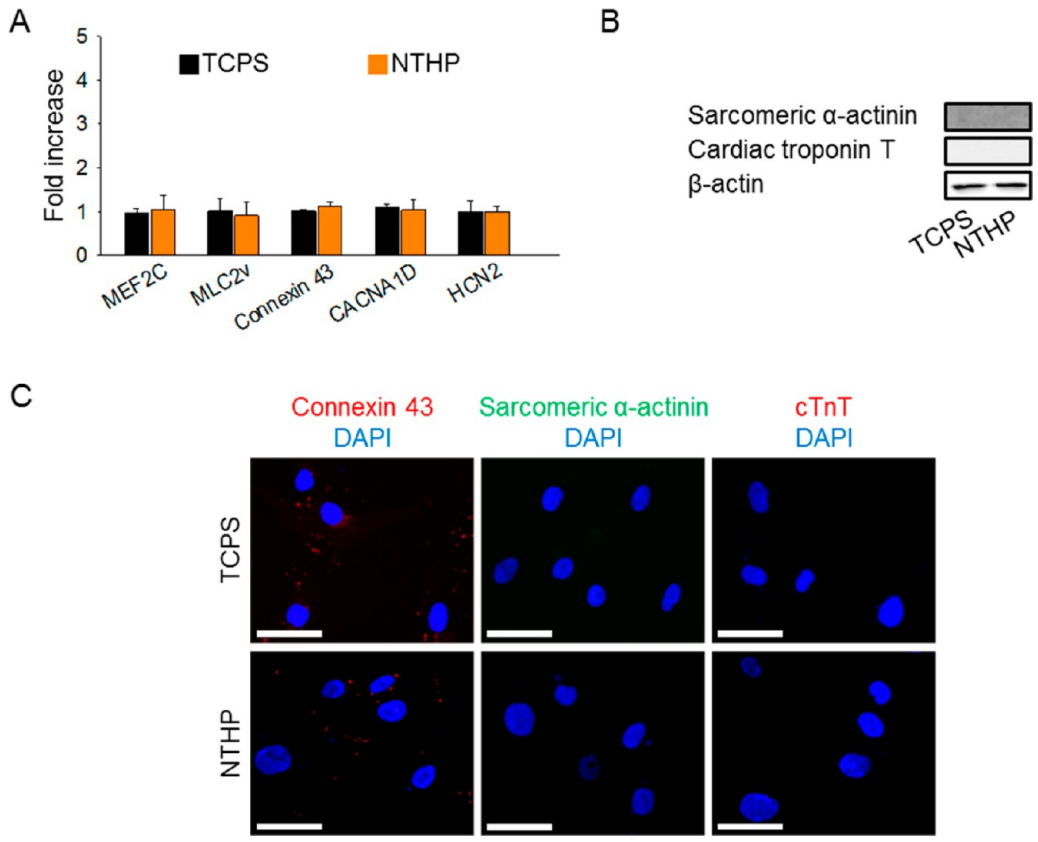

Figure 7. Effects of NTHP membrane on cardiac differentiation of MSCs without coculture. (A) mRNA expression levels of cardiac transcription factor (MEF2C), cardiac structural marker (MLC2v), gap junction marker (connexin 43), and cardiac ion channel markers (CACNA1D, HCN2) in MSCs after 1 week culture on tissue culture plate dishes (TCPS) or NTHP membrane (NTHP) without coculture. Gene expression levels were normalized to the levels of MSCs cultured on TCPS. (B) Western blot analyses for cardiac structural proteins, sarcomeric α-actinin and cardiac troponin T of MSCs after culture for 1 week. (C) Immunocytochemistry for cardiac protein markers of MSCs after culture for 1 week. Bars, 50 μm.

Western blot analysis (Figure 5B) and immunocytostaining (Figure 5C) of noncocultured MSCs showed no expression of the cardiac structural proteins, sarcomeric α-actinin (SA) and cardiac troponin T (cTnT). The same results were observed in Transwell (Indirect). Meanwhile, Transwell (Direct) showed slightly increased expression of SA protein. In contrast, NTHP demonstrated significantly higher expressions of both SA and cTnT proteins compared to other groups. Also, NTHP showed a higher expression of connexin-43 compared to the other groups. Statistically, the percentages of MSCs that were positive for cardiac-specific markers were significantly higher in the NTHP group than the other groups (Figure 5C). The cardiac differentiation efficiency of MSCs in the NTHP membrane coculture system was comparable to that of MSCs directly cocultured with H9C2s without the NTHP membrane (Figure 6). Additionally, we cultured MSCs on their own on NTHP membranes and confirmed that the membrane itself does not affect their differentiation (Figure 7). These results showed that NTHP membranes improve the cardiac differentiation efficiency of MSCs compared to other coculture systems, which is likely due to the dynamic cell-to-cell interactions between the cell populations in this membrane system. While a number of previous studies attempted to induce terminal cardiac differentiation of MSCs, functional cardiac behaviors such as contractility have not been observed in the differentiated cells.[10,46,47,49−53] Also, previous studies indicated that H9C2s cardiomyoblast cell line lacks many ion currents typical of the mature heart and shows no voltage-dependent current.[54,55] Hence, based on the aforementioned reports, the present study did not address the contractility of the differentiated cell sheets.

Generation of Transfer-Printable, Multilayered Sheets of Differentiated Cells. The transferable and thermoresponsive features of NTHP membranes allow the generation of transfer-printable, multilayered sheets of differentiated cells after coculture. Cell sheet printing can be achieved by turning the thermoresponsive NTHP membrane upside down, allowing the cell sheet to adhere to a new culture dish at 37 °C for 4 h, and printing the cell sheet onto the culture dish from the membrane at 20 °C for 30 min. Repeating the transfer-printing of a new cell sheet layer on top of the first transfer-printed cell sheet layer can be used to fabricate multilayered sheets of differentiated cells (Figure 8A).

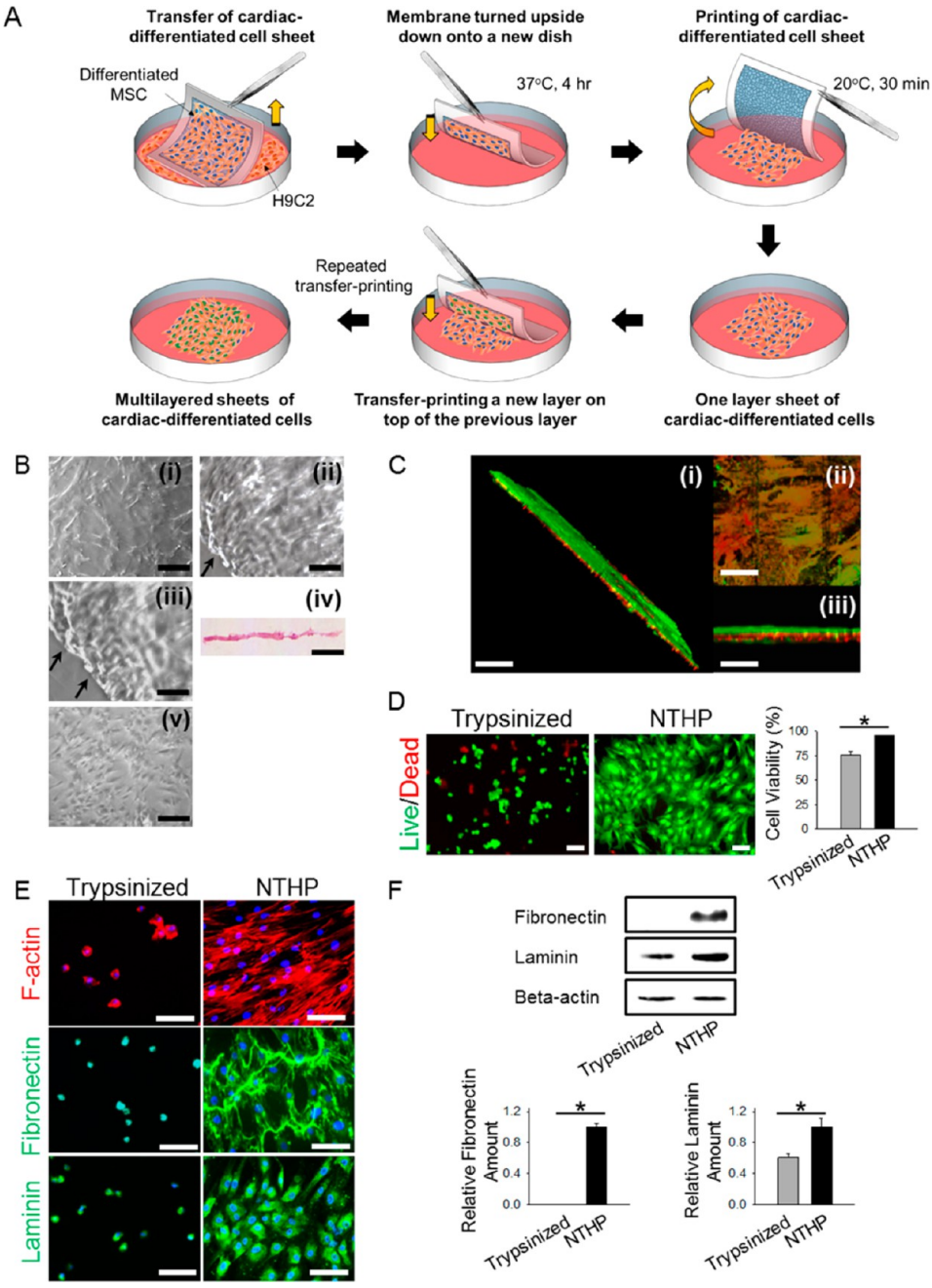

Figure 8. Generation of bilayered cells sheets by the transfer-printing technique using a thermoresponsive NTHP membrane, and characterization of the cells sheets. (A) Schematic diagram of the generation of multilayered cell sheets with the transfer-printing technique using NTHP membranes. (B) Light microscopic images of (i) a cell sheet adhering on NTHP membrane at 37 °C, (ii) a cell sheet gradually detaching from NTHP membrane after 20 min at 20 °C, and (iii) after 30 min at 20 °C, (iv) cross-sectional view of the detached membrane, (iv) H&E stained cell sheet, and (v) transfer-printed cell sheet on a new culture dish. Cell sheet detachment is marked with arrows. Bars, 100 μm. (C) z-Stack confocal images of bilayered cell sheets generated by the transfer-printing technique using NTHP membranes viewed from (i) 3D tilt angle, (ii) top, and (iii) side. A second layer (green) of cell sheet was stacked on top of the first layer (red) of cell sheet. Bars, 100 μm. (D) Cell viability assessment and quantification after trypsinization or transfer-printing, as evaluated by live (green)/dead (red) assay. Bars, 100 μm. *$p < 0.05$. (E) Immunofluorescent images of actin cytoskeleton (F-actin) and ECM (fibronectin and laminin) proteins expressed in trypsinized (dissociated) single cells and a transfer-printed cell sheet. DAPI stained nuclei. Bars, 100 μm. (F) Western blot analyses of ECM proteins in trypsinized single cells and transfer-printed cell sheet. *$p < 0.05$.

Light microscopy images capturing the transfer printing process are shown in Figure 8B. A transferred NTHP membrane showed MSCs firmly adhered to the membrane (Figure 8Bi). Gradually, the cells started to detach from the NTHP membrane at 20 °C within 20 min, starting from the edge of the membrane (Figure 8Bii), followed by extensive detachment of the cell sheet within 30 min (Figure 8Biii). A cross-sectional view of the detached cell sheet stained by hematoxylin and eosin (H&E) displayed an intact monolayer cell sheet

(Figure 8Biv). In addition, we demonstrated that it was possible to print the transferred and detached cell sheet onto a new culture dish (Figure 8Bv).

Next, to determine whether the transfer-printing technique with the thermoresponsive NTHP membrane can be used to fabricate multilayered cell sheets, consecutive cell sheets transfer-printing was performed. Prior to transfer-printing, each cell sheet was prelabeled using red (DiI) or green (DiO) fluorescence dyes, respectively. The transfer-printing technique with the thermoresponsive NTHP membrane was performed by stacking a red fluorescent-labeled cell sheet onto a green fluorescent-labeled cell sheet, resulting in the fabrication of a bilayered cell sheet (Figure 8C). The z-stack 3D confocal images of the bilayered cell sheets showed intact incorporation between the layers (Figure 8C).

Detachment of the cell sheet from a thermoresponsive substrate is reported to be an advanced approach to harvesting adherent cultured cells compared to the conventional method using trypsin.[56,57] Trypsin, a proteolytic enzyme that degrades ECM proteins, is known to have harmful effects on the viability of the trypsinized cells, since these proteins are crucial components of the cellular microenvironment for cell survival.[20,58] To examine the cell viability of the transfer-printed cell-sheet generated with thermoresponsive NTHP membranes, a live (green)/dead (red) cell staining assay was performed and compared with cells harvested by trypsinization. The data showed that cells recovered using trypsin treatment showed only 75% cell viability, while transfer-printed cell sheets by NTHP membranes showed higher cell viability, up to 96% (Figure 8D).

In addition, while actin cytoskeleton staining of the trypsinized cells showed dissociated single cells after cell harvesting, the transfer-printed cell sheet was intact (Figure 8E). Immunocytostaining and Western blot analysis of ECM molecules of the transfer-printed cell sheets were also examined and compared with cells harvested by trypsinization. Notably, ECM proteins, such as fibronectin and laminin, were better preserved in the NTHP membrane-generated cell sheet compared to trypsinized cells (Figure 8E and Figure 8F). The data confirmed that transfer-printed cell sheets generated using thermoresponsive NTHP membranes had a higher survival rate and better preserved ECM proteins compared to the conventional cell-harvesting method.

CONCLUSIONS

We developed nanothin, highly porous, and thermoresponsive membranes for the generation of transfer-printable, stem cell-derived, multilayered cardiac sheets. The feasibility of using NTHP membranes as an effective substrate for coculture was confirmed by the demonstration of the biocompatibility of the membrane, direct cell−cell contact between MSC-H9C2s, fast protein diffusion across the membrane, and enhanced cardiac differentiation of MSCs following coculture. The precise control of the pore architecture of NTHP membranes at the nanoscale level enabled a systematic search for the most efficient pore size for stem cell coculture. The tunable pore dimension was a key parameter in regulating cell-to-cell communication, ranging from diffusion of soluble paracrine factors to direct gap junction-mediated cell-to-cell contacts, and preventing cellular cross-migrations between the cocultured cell populations. In addition, thermoresponsive NTHP membranes enabled the facile engineering of multilayered cell sheets by the transfer-printing technique.

The novel development of a customized and tunable NTHP membrane-based system will serve as an efficient coculture platform that can regulate the cell-to-cell interactions between the cocultured cells. Also, this platform might prove useful for engineering various types of functional tissues by coculturing stem cells and the desired type of differentiated cells. Since this system can potentially be used to differentiate patient-derived stem cells, it opens up the possibility for patient-specific, personalized drug testing and toxicological studies.

MATERIALS AND METHODS

Fabrication of NTHP Membrane. Cellulose acetate (CA) with an average molecular weight (M_n) of 30 000 g/mol (39.8 wt % acetyl labeling extent) was prepared (Sigma-Aldrich Co., USA). CA was dissolved in a good solvent, THF, at 4 wt % for NTHP-380 membranes. For NTHP-860 membranes, 3 wt % CA was dissolved in THF, and acetone was used as a solvent for fabricating NTHP-100 membranes. NTHP membranes were deposited onto silicon (Si) wafers, which were previously cleaned by dipping in a piranha solution, a mixture of 70 vol % H_2SO_4 and 30 vol % H_2O_2, for 20 min at room-temperature, then rinsed with deionized (DI) water and dried with a nitrogen stream. To obtain the nanoporous structure of NTHP membranes, the spin-casting of CA solutions onto Si wafers was performed with a spinning rate of 3000 rpm (NTHP-100 and NTHP-380) or 1000 rpm (NTHP-860) for 25 s, using an automatic spin coater in a closed humid chamber with controlled RH. Since CA polymers are not soluble in water, the porous structure in NTHP membranes was developed using a VIPS mechanism, and the pore size was controlled by the RH in the closed chamber packed with different types of supersaturated salt solutions (KCl for RH 55−85%). For the NTHP membranes used in our experiment, we set up the RH to 65 ± 5% (NTHP-100 and NTHP-380), and 55 ± 5% (NTHP-860). The freestanding NTHP membranes were obtained by peeling off the membranes from the Si wafers in water after efficiently drying the samples. We modified the NTHP membranes using the method proposed by Ku *et al.*[59] to enhance cell adhesion. NTHP membranes were coated in a dopamine hydrochloride solution for up to 16 h. Dopamine hydrochloride (Sigma-Aldrich Co.) was dissolved in 10 mM Tris buffer at 2 mg/mL, and the pH was adjusted to 8.5 using dilute NaOH solution. A PET film was used as a frame for easier handling of the NTHP membranes. The PET-frame was fixed with UV-curable poly(urethane

acrylate) (PUA, 311-RM, Minuta Tech, Korea), which acts as a glue. The PUA was irradiated with UV (λ = 365 nm) for 3 h.

PNIPAAm Grafting onto NTHP Membrane for Temperature-Responsive Property. GMA monomer (97%) and the *tert*-butyl peroxide (TBPO) initiator (98%) were purchased from Sigma-Aldrich and used without further purification. Polymerized GMA films were deposited onto the NTHP membranes in an iCVD reactor (Daeki Hi-Tech Co., Korea). The GMA monomer was heated to 35 °C and the vaporized GMA was fed into the reactor at a flow rate of 1.9 sccm for coating the pGMA film on the NTHP membrane. The vaporized TBPO initiator was fed into the reactor *via* metering valves at a flow rate of 0.8 sccm at room-temperature. To keep the NTHP membrane at 25 °C during the pGMA coating process, the membranes were placed on a stage cooled by a recirculating chiller. The filament temperature was maintained at 180 °C. The growth rate of film deposition was monitored *in situ* using a He−Ne laser (JDS Uniphase, Milpitas, USA). Amine-terminated PNIPAAm (Mn = 2500, Sigma-Aldrich Co.) was dissolved in deionized (DI) water at a concentration of 1 g/30 mL. The PNIPAAm solution was reacted with the pGMA deposited NTHP membrane through epoxy-amine addition reaction in a shaker at 50 °C for 12 h at 55 rpm. Next, it was washed several times with DI water. Prior to cell seeding, membranes were sterilized with 70% (v/v) ethanol and UV treated for 1 h on a clean bench.

Characterization of NTHP Membranes. The surface morphologies of NTHP membranes were characterized by scanning electron microscopy (SEM, JSM-6701F, JEOL, Japan) and atomic force microscopy (AFM, JPK, Nanowizard 3, Germany, and diInnova, Veeco, USA). The thicknesses of the NTHP membranes were measured using a step height measurement (AlphaStep IQ (revision A1-1), KLA-Tencor, USA). Based on previous studies, both SEM and AFM images were used to determine the average pore sizes of the NTHP membranes.[60,61] Pore size represents the average value of the shortest and the longest axes of each pore. The porosity of each membrane was analyzed using an image processing software, ImageJ (National Institutes of Mental Health, USA). AFM images were adjusted to black/white binary phase, and then the proportion of white area to the total area was considered as the porosity of the membrane. Fourier transform infrared spectroscopy (FT-IR, IFS 66VS, Bruker, Billerica, USA) spectra were obtained in normal absorbance mode and averaged over 64 scans in order to confirm PNIPAAm functionalization. X-ray photoelectron spectroscopy (XPS, MultiLab 2000, Thermo, USA) was also utilized to determine surface chemical composition of NTHP membranes. Water contact angle measurements were made using a contact angle meter (Phoenix 150, SEO, Korea) with a 2.5 μL DI water droplet. The contact angle meter was equipped with an environment chamber to control the temperature range from 25 to 250 °C.

Cell Culture. Human bone marrow-derived mesenchymal stem cells (MSCs) were purchased from a commercial source (Lonza, USA), and H9C2s, a rat cardiac myoblast cell line, were purchased from Korean Cell Line Bank (Korea). Prior to coculture, both MSCs and H9C2s were cultured in growth medium consisting of high-glucose Dulbecco's modified Engle's Medium (DMEM; Gibco BRL, USA) containing 10% (v/v) fetal bovine serum (FBS; Gibco-BRL) and 1% (v/v) penicillin-streptomycin (PS; Gibco-BRL) at 37 °C in humid air with 5% CO_2.

Cell Viability and Proliferation. For cell viability and proliferation studies, MSCs were seeded at a density of 3×10^3 cells/cm^2 on tissue culture polystyrene (TCPS) dishes, Transwell membranes (pore size 400 nm), and NTHP membranes (pore size 380 nm). Transwell culture inserts for six-well plates (0.4 μm pore, polyester membrane) were purchased from a commercial source (Corning, USA). The viable cell number was determined using Cell Counting Kit-8 assay (CCK-8, Sigma-Aldrich Co.) (n = 3 per groups). The gene expression levels of BAX and Bcl-2 in MSCs were determined by qRT-PCR to assess the expression of apoptotic and antiapoptotic genes, respectively (n = 3 per group). The proliferating cells were evaluated by immunocytochemistry using antibodies against PCNA. The samples were mounted in 4,6-diamidino-2-phenylindole (DAPI, Vector Laboratories, USA) for nuclear staining. Each image was photographed using a fluorescence microscope (IX71 inverted microscope, Olympus, Japan). The numbers of PCNA-positive cells were digitally quantified (n = 10 images per group) using Image Pro Plus software (Media Cybernetics, UK).

Coculture of MSCs and H9C2s Cells. For the coculture of MSCs and H9C2s using NTHP membranes, H9C2s were plated at a density of 2×10^3 cells/cm^2 on TCPS dishes, and MSCs were plated at a density of 3×10^3 cells/cm^2 on NTHP membranes. The following day, the MSC-seeded NTHP membrane was layered on top of the H9C2-seeded TCPS dish. To prevent the layered membrane from moving, a square stainless steel ring was placed on top of the NTHP membrane. Two coculture methods using the Transwell system, that is, indirect and direct coculture, were used for comparison. In indirect coculture, H9C2s were seeded on a Transwell insert and MSCs were seeded on the lower six-well plate compartment. In direct coculture, MSCs were seeded on the bottom side of the Transwell membrane. The following day, H9C2s were seeded on the other (top) side of the Transwell membrane. In the direct coculture group, without any membrane, DiI-labeled (6.25 μg/mL; Sigma-Aldrich Co.) H9C2s and nonlabeled MSCs were cocultured with no barrier between the heterogeneous cells, at the same initial cell number ratio (H9C2/MSC = 2:3), as other groups. Prior to evaluating differentiation efficiency, cocultured MSCs were separated from DiI-labeled H9C2s by fluorescence-activated cell sorting (FACS Aria II BD Biosciences, USA). For noncocultured control groups, MSCs were cultured on TCPS dishes or NTHP membranes. The medium was changed every 2 days.

Interactions between the Cocultured Cells. The proximities between MSCs and H9C2s cocultured on the two sides of the NTHP membranes with different pore sizes and the Transwell membranes were observed by prelabeling the MSCs with DiO (6.25 μg/mL; Sigma-Aldrich Co., USA) and H9C2s with DiI (6.25 μg/mL; Sigma-Aldrich Co.), prior to coculture. Images were captured using a confocal microscope (SP8 X STED, super-resolution confocal microscope, Leica, Germany) after 48 h of coculture. For the dye transfer assay, MSCs were dual-labeled with DiI (Sigma-Aldrich Co.) and calcein-AM (Sigma-Aldrich Co.). MSCs on TCPS were incubated in DiI working solution (6.25 μg/mL) for 2 h at 37 °C and then rinsed with culture medium three times to wash off excess DiI. Next, the MSCs were incubated in serum-free culture medium containing calcein-AM (10 μmol/L, a cell-permeable ester form of calcein) for 30 min at 37 °C, and rinsed with PBS three times to wash off the extracellular calcein-AM. Subsequently, the dual-labeled MSCs were trypsinized and plated on NTHP membrane. The MSC-seeded NTHP membrane was layered on top of H9C2-seeded glass-bottom culture dishes (Corning). Images were captured after 48 h of coculture using a confocal microscope (SP8 X STED, super-resolution confocal microscope, Leica) to investigate dye transfer from MSCs to H9C2s. The dye transfer assay was performed based on previous studies.[35,38,39] To determine the rate of protein diffusion through the NTHP and Transwell membranes, a protein diffusion chamber was designed. A Transwell or NTHP membrane was used to partition the protein diffusion chamber into two secluded compartments filled with 10 mL of 10 μg/mL bovine serum albumin (BSA, Sigma-Aldrich Co.) solution on one side and phosphate buffer saline (PBS, Sigma-Aldrich Co.) of equal volume on the other side. Samples were collected from the PBS chamber at various time points, and the concentrations of BSA in the samples were quantified using the Bradford protein assay (n = 3 per group) (Sigma-Aldrich Co.).

Homogeneity of the Collected MSCs Postcoculture. Prior to coculture, MSCs were prelabeled with DiO (6.25 μg/mL; Sigma-Aldrich Co.) and H9C2s with DiI (6.25 μg/mL; Sigma-Aldrich Co.). After coculturing for 1 week, images of the cocultured MSCs and H9C2s were captured using a fluorescence microscope (IX71 inverted microscope, Olympus). In addition, images of the MSCs harvested from the transfer of MSC-seeded NTHP membranes (380 nm pore size) onto new culture dishes after coculturing for 1 week, were photographed using a fluorescence microscope (IX71 inverted microscope, Olympus). To assess the purity of the collected cells, cells adhered to the transferred NTHP membranes were trypsinized and evaluated by fluorescence-activated cell sorting (FACS Aria II BD Biosciences, USA) installed at the National Center for Interuniversity

Research Facilities (NCIRF) at Seoul National University and fluorescence microscopy (IX71 inverted microscope, Olympus) (n = 10 images per group). MSCs collected from the Transwell direct coculture group *via* trypsinization.

Differentiation of MSCs After Coculture for 1 Week. The expressions of cardiac-specific genes in MSCs were evaluated using qRT-PCR. RNA was extracted from MSCs and reverse-transcribed into cDNA. Expression of a cardiac transcription factor (MEF2C), a cardiac structural marker (MLC2v), a gap junction marker (connexin 43), and cardiac ion channel markers (CACNA1D, HCN2) were evaluated using StepOnePlus real-time PCR system (Applied Biosystems, USA) with FAST SYBR Green PCR Master Mix (Applied Biosystems) for 45 cycles. Each cycle consisted of the following temperatures and times: 94 °C for 3 s and 60 °C for 30 s (n = 3 per group). For protein detection, Western blot analysis on sarcomeric α-actininin and cardiac troponin T were performed. In addition, immunocytochemistry for connexin-43, sarcomeric α-actininin, and cardiac troponin T was performed. The numbers of sarcomeric α-actininin-positive cells and cardiac troponin T-positive cells were digitally quantified (n = 10 images per group) using Image Pro Plus software (Media Cybernetics, UK).

Transfer-Printing of Cell Sheet. Cell sheet printing was achieved by transferring an MSC-seeded, thermoresponsive NTHP membrane onto a new culture dish and changing the temperature. The MSC-seeded membrane was turned upside down and incubated for 4 h at 37 °C, allowing the cell sheet to adhere to the new culture dish. Printing was then induced by incubating the membrane for 30 min at 20 °C. Cell sheet printing was observed under a light microscope (IX71 inverted microscope, Olympus). For histological analysis, the printed cell sheet was embedded in Optimal Cutting Temperature (OCT) compound (Sakura Finetek, USA), frozen, and cut (10 μm in thickness) using a cryostat cryocut microtome (Leica, CM3050S, Germany). After hematoxylin and eosin (H&E) staining, the stained cross sections of the cell sheet were examined by light microscopy (IX71 inverted microscope, Olympus). The viability of the cells harvested *via* transfer-printing was compared to that of trypsinized cells by assessing the nmber of live and dead cells using calcein-AM and ethidium homodimer, respectively. A two-color fluorescence live/dead assay kit (Molecular Probes, USA) (n = 10 images per group) was used for analysis. To analyze the extracellular matrices of the transfer-printed cell sheet, immunocytochemical staining for fibronectin and laminin was performed. In addition, Western blot analyses on laminin and fibronectin were performed (n = 3). For examination of bilayered cell sheets, prior to transfer-printing, each cell sheet was prelabeled with DiI (6.25 μg/mL; Sigma-Aldrich Co.) or DiO (6.25 μg/mL; Sigma-Aldrich Co.). Subsequently, transfer-printing was performed and the DiI-labeled cell sheet was stacked on the DiO-labeled cell sheet. The z-stack 3D confocal images of the bilayered cell sheets were obtained using a confocal microscope (SP8 X STED, super-resolution confocal microscope, Leica).

Western Blot Analysis. Cell lysate was prepared using cell lysis buffer (Cell Signaling, U.S.A). The total concentration of the protein was determined using the Bradford protein assay (Sigma-Aldrich Co.) prior to loading the samples on a 10% (w/v) SDS−polyacrylamide gel. Proteins were transferred to Immobilon-P membrane (Millipore Corp., USA), blocked with 5% skimmed milk solution for 1 h at room-temperature, and incubated with antibodies against sarcomeric α-actininin (Abcam, UK), cardiac troponin T (Abcam), fibronectin (Abcam), and laminin (Abcam) overnight at 4 °C. The membrane was incubated with horseradish peroxidase-conjugated secondary antibody (Santa Cruz Biotechnology, USA) for 1 h at room-temperature. The blots were developed using a chemiluminescence detection system (Amersham Bioscience, USA).

Cell Staining. Cells and cell sheets were fixed in 4% paraformaldehyde solution, permeabilized with 0.1% Triton X-100, and then blocked with 1% BSA for 1 h for actin filament staining. The actin filaments of the cells were stained by tetramethylrhodamine isothiocyanate (TRITC)-conjugated phalloidin (1:40; Molecular Probes, USA). For immunocytochemical staining, cells were fixed in 4% paraformaldehyde solution, permeabilized with 0.6% Triton X-100 and then blocked with 10% donkey serum (Jackson ImmunoResearch Laboratories, USA). The samples were then reacted with antibody against PCNA (produced in rabbit, 10 μg/mL; Abcam), cardiac troponin T (produced in mouse, 1/400; Abcam), connexin 43 (produced in rabbit, 1:1000; Abcam), sarcomeric α-actinin (produced in rabbit, 1/200; Abcam), fibronectin (produced in rabbit, 1/500; Abcam), and laminin (produced in rabbit, 1/100; Abcam). PCNA, cardiac troponin T, and connexin 43 staining were detected with tetramethylrhodamine isothiocyanate-conjugated secondary antibodies (Jackson ImmunoResearch Laboratories). Sarcomeric α-actinin, fibronectin, and laminin staining were detected with fluorescein isothiocyanate-conjugated secondary antibodies (Jackson ImmunoResearch Laboratories). The samples were mounted in 4,6-diamidino-2-phenylindole (DAPI, Vector Laboratories, USA) for nuclear staining. Fluorescence images were captured using a fluorescence microscope (IX71 inverted microscope, Olympus, Japan).

Statistical Analysis. Quantitative data were expressed as the means plus or minus the standard deviations. The statistical analysis was performed using one-way analysis of variance (ANOVA) with the Tukey's significant difference *post hoc* test using SPSS software (SPSS Inc., USA). A value of $p < 0.05$ was considered as statistically significant.

Conflict of Interest: The authors declare no competing financial interest.

Acknowledgment. This research was supported by the National Creative Research Initiative Center for Intelligent Hybrids (No. 2010-0018290) funded by the National Research Foundation of Korea, and the Korea Health Industry Development Institute (HI14C1550 and HI15C0498) funded by the Ministry of Health and Welfare, Republic of Korea.

Supporting Information Available: The Supporting Information is available free of charge on the ACS Publications website at DOI: 10.1021/acsnano.5b03823.

Pore size distributions; FT-IR spectra; calculations; additional figures and table (PDF)

REFERENCES AND NOTES

1. Mooney, D. J.; Vandenburgh, H. Cell Delivery Mechanisms for Tissue Repair. *Cell stem cell* **2008**, *2*, 205–213.
2. Hyun, J. S.; Tran, M. C.; Wong, V. W.; Chung, M. T.; Lo, D. D.; Montoro, D. T.; Wan, D. C.; Longaker, M. T. Enhancing Stem Cell Survival *in Vivo* for Tissue Repair. *Biotechnol. Adv.* **2013**, *31*, 736–743.
3. Beeres, S. L.; Zeppenfeld, K.; Bax, J. J.; Dibbets-Schneider, P.; Stokkel, M. P.; Fibbe, W. E.; van der Wall, E. E.; Atsma, D. E.; Schalij, M. J. Electrophysiological and Arrhythmogenic Effects of Intramyocardial Bone Marrow Cell Injection in Patients with Chronic Ischemic Heart Disease. *Heart rhythm* **2007**, *4*, 257–265.
4. Morrison, S. J.; Spradling, A. C. Stem Cells and Niches: Mechanisms That Promote Stem Cell Maintenance Throughout Life. *Cell* **2008**, *132*, 598–611.
5. Lee, S. H.; Shin, H. Matrices and Scaffolds for Delivery of Bioactive Molecules in Bone and Cartilage Tissue Engineering. *Adv. Drug Delivery Rev.* **2007**, *59*, 339–59.
6. Park, H.; Temenoff, J. S.; Tabata, Y.; Caplan, A. I.; Mikos, A. G. Injectable Biodegradable Hydrogel Composites for Rabbit Marrow Mesenchymal Stem Cell and Growth Factor Delivery for Cartilage Tissue Engineering. *Biomaterials* **2007**, *28*, 3217–27.
7. Ryu, S.; Lee, C.; Park, J.; Lee, J. S.; Kang, S.; Seo, Y. D.; Jang, J.; Kim, B. S. Three-Dimensional Scaffolds of Carbonized Polyacrylonitrile for Bone Tissue Regeneration. *Angew. Chem., Int. Ed.* **2014**, *53*, 9213–7.
8. Hwang, N. S.; Varghese, S.; Elisseeff, J. Controlled Differentiation of Stem Cells. *Adv. Drug Delivery Rev.* **2008**, *60*, 199–214.
9. Kay Sinclair, S. S.; Burg, K. J. Effect of Osteoclast Co-Culture on the Differentiation of Human Mesenchymal Stem Cells

Grown on Bone Graft Granules. *J. Biomater. Sci., Polym. Ed.* **2011**, *22*, 789–808.
10. Fukuhara, S.; Tomita, S.; Yamashiro, S.; Morisaki, T.; Yutani, C.; Kitamura, S.; Nakatani, T. Direct Cell-Cell Interaction of Cardiomyocytes Is Key for Bone Marrow Stromal Cells to Go into Cardiac Lineage *in Vitro*. *J. Thorac. Cardiovasc. Surg.* **2003**, *125*, 1470–1479.
11. Yen, B. L.; Chien, C.-C.; Chen, Y.-C.; Chen, J.-T.; Huang, J.-S.; Lee, F.-K.; Huang, H.-I. Placenta-Derived Multipotent Cells Differentiate into Neuronal and Glial Cells *in Vitro*. *Tissue Eng., Part A* **2008**, *14*, 9–17.
12. Kiger, A. A.; White-Cooper, H.; Fuller, M. T. Somatic Support Cells Restrict Germline Stem Cell Self-Renewal and Promote Differentiation. *Nature* **2000**, *407*, 750–754.
13. Battiston, K. G.; Cheung, J. W.; Jain, D.; Santerre, J. P. Biomaterials in Co-Culture Systems: Towards Optimizing Tissue Integration and Cell Signaling within Scaffolds. *Biomaterials* **2014**, *35*, 4465–4476.
14. Agrawal, A. A.; Nehilla, B. J.; Reisig, K. V.; Gaborski, T. R.; Fang, D. Z.; Striemer, C. C.; Fauchet, P. M.; McGrath, J. L. Porous Nanocrystalline Silicon Membranes as Highly Permeable and Molecularly Thin Substrates for Cell Culture. *Biomaterials* **2010**, *31*, 5408–5417.
15. Kim, S.; Ahn, S. E.; Lee, J. H.; Lim, D. S.; Kim, K. S.; Chung, H. M.; Lee, S. H. A Novel Culture Technique for Human Embryonic Stem Cells Using Porous Membranes. *Stem Cells* **2007**, *25*, 2601–2609.
16. Pandiyan, P.; Zheng, L.; Ishihara, S.; Reed, J.; Lenardo, M. J. Cd4+ Cd25+ Foxp3+ Regulatory T Cells Induce Cytokine Deprivation−Mediated Apoptosis of Effector Cd4+ T Cells. *Nat. Immunol.* **2007**, *8*, 1353–1362.
17. Sekine, H.; Shimizu, T.; Dobashi, I.; Matsuura, K.; Hagiwara, N.; Takahashi, M.; Kobayashi, E.; Yamato, M.; Okano, T. Cardiac Cell Sheet Transplantation Improves Damaged Heart Function *Via* Superior Cell Survival in Comparison with Dissociated Cell Injection. *Tissue Eng., Part A* **2011**, *17*, 2973–2980.
18. Ohashi, K.; Yokoyama, T.; Yamato, M.; Kuge, H.; Kanehiro, H.; Tsutsumi, M.; Amanuma, T.; Iwata, H.; Yang, J.; Okano, T.; et al. Engineering Functional Two-and Three-Dimensional Liver Systems *in Vivo* Using Hepatic Tissue Sheets. *Nat. Med.* **2007**, *13*, 880–885.
19. Matsuda, N.; Shimizu, T.; Yamato, M.; Okano, T. Tissue Engineering Based on Cell Sheet Technology. *Adv. Mater.* **2007**, *19*, 3089–3099.
20. Miyahara, Y.; Nagaya, N.; Kataoka, M.; Yanagawa, B.; Tanaka, K.; Hao, H.; Ishino, K.; Ishida, H.; Shimizu, T.; Kangawa, K.; et al. Monolayered Mesenchymal Stem Cells Repair Scarred Myocardium after Myocardial Infarction. *Nat. Med.* **2006**, *12*, 459–465.
21. Haraguchi, Y.; Shimizu, T.; Sasagawa, T.; Sekine, H.; Sakaguchi, K.; Kikuchi, T.; Sekine, W.; Sekiya, S.; Yamato, M.; Umezu, M.; et al. Fabrication of Functional Three-Dimensional Tissues by Stacking Cell Sheets *in Vitro*. *Nat. Protoc.* **2012**, *7*, 850–858.
22. Sekiya, N.; Matsumiya, G.; Miyagawa, S.; Saito, A.; Shimizu, T.; Okano, T.; Kawaguchi, N.; Matsuura, N.; Sawa, Y. Layered Implantation of Myoblast Sheets Attenuates Adverse Cardiac Remodeling of the Infarcted Heart. *J. Thorac. Cardiovasc. Surg.* **2009**, *138*, 985–993.
23. Iwata, T.; Yamato, M.; Tsuchioka, H.; Takagi, R.; Mukobata, S.; Washio, K.; Okano, T.; Ishikawa, I. Periodontal Regeneration with Multi-Layered Periodontal Ligament-Derived Cell Sheets in a Canine Model. *Biomaterials* **2009**, *30*, 2716–2723.
24. Annamalai, P. K.; Pochat-Bohatier, C.; Bouyer, D.; Li, C. L.; Deratani, A.; Wang, D. M. Kinetics of Mass Transfer During Vapour-Induced Phase Separation (Vips) Process and Its Influence on Poly-(Vinylidene Fluoride) (Pvdf) Membrane Structure and Surface Morphology. *Desalin. Water Treat.* **2011**, *34*, 204–210.
25. Li, M.; Katsouras, I.; Piliego, C.; Glasser, G.; Lieberwirth, I.; Blom, P. W. M.; de Leeuw, D. M. Controlling the Microstructure of Poly(Vinylidene-Fluoride) (Pvdf) Thin Films for Microelectronics. *J. Mater. Chem. C* **2013**, *1*, 7695.
26. Venault, A.; Chang, Y.; Wang, D.-M.; Bouyer, D. A Review on Polymeric Membranes and Hydrogels Prepared by Vapor-Induced Phase Separation Process. *Polym. Rev.* **2013**, *53*, 568–626.
27. Yamato, M.; Okano, T. Cell Sheet Engineering. *Mater. Today* **2004**, *7*, 42–47.
28. Cole, M. A.; Voelcker, N. H.; Thissen, H.; Griesser, H. J. Stimuli-Responsive Interfaces and Systems for the Control of Protein−Surface and Cell−Surface Interactions. *Biomaterials* **2009**, *30*, 1827–1850.
29. Kushida, A.; Yamato, M.; Konno, C.; Kikuchi, A.; Sakurai, Y.; Okano, T. Decrease in Culture Temperature Releases Monolayer Endothelial Cell Sheets Together with Deposited Fibronectin Matrix from Temperature-Responsive Culture Surfaces. *J. Biomed. Mater. Res.* **1999**, *45*, 355–362.
30. Akiyama, Y.; Kikuchi, A.; Yamato, M.; Okano, T. Ultrathin Poly (N-Isopropylacrylamide) Grafted Layer on Polystyrene Surfaces for Cell Adhesion/Detachment Control. *Langmuir* **2004**, *20*, 5506–5511.
31. Masuda, S.; Shimizu, T.; Yamato, M.; Okano, T. Cell Sheet Engineering for Heart Tissue Repair. *Adv. Drug Delivery Rev.* **2008**, *60*, 277–285.
32. Im, S. G.; Gleason, K. K. Solvent-Free Modification of Surfaces with Polymers: The Case for Initiated and Oxidative Chemical Vapor Deposition (Cvd). *AIChE J.* **2011**, *57*, 276–285.
33. Kim, M.-J.; Lee, B.; Yang, K.; Park, J.; Jeon, S.; Um, S. H.; Kim, D.-I.; Im, S. G.; Cho, S.-W. Bmp-2 Peptide-Functionalized Nanopatterned Substrates for Enhanced Osteogenic Differentiation of Human Mesenchymal Stem Cells. *Biomaterials* **2013**, *34*, 7236–7246.
34. Park, H. J.; Yu, S. J.; Yang, K.; Jin, Y.; Cho, A. N.; Kim, J.; Lee, B.; Yang, H. S.; Im, S. G.; Cho, S. W. Paper-Based Bioactive Scaffolds for Stem Cell-Mediated Bone Tissue Engineering. *Biomaterials* **2014**, *35*, 9811–23.
35. Han, J.; Kim, B.; Shin, J.-Y.; Ryu, S.; Noh, M.; Woo, J.; Park, J.-S.; Lee, Y.; Lee, N.; Hyeon, T.; et al. Iron Oxide Nanoparticle-Mediated Development of Cellular Gap Junction Crosstalk to Improve Mesenchymal Stem Cells' Therapeutic Efficacy for Myocardial Infarction. *ACS Nano* **2015**, *9*, 2805–2819.
36. Saltzman, W. M.; Langer, R. Transport Rates of Proteins in Porous Materials with Known Microgeometry. *Biophys. J.* **1989**, *55*, 163–71.
37. Guo, Y.; O'Donohue, S. J.; Langley, K. H.; Karasz, F. E. Polymer Diffusion in Porous Media of Fumed Silica Studied by Forced Rayleigh Scattering. *Phys. Rev. A: At., Mol., Opt. Phys.* **1992**, *46*, 3335.
38. Haraguchi, Y.; Shimizu, T.; Yamato, M.; Kikuchi, A.; Okano, T. Electrical Coupling of Cardiomyocyte Sheets Occurs Rapidly *Via* Functional Gap Junction Formation. *Biomaterials* **2006**, *27*, 4765–4774.
39. Lampe, P. D. Analyzing Phorbol Ester Effects on Gap Junctional Communication: A Dramatic Inhibition of Assembly. *J. Cell Biol.* **1994**, *127*, 1895–1905.
40. Makino, S.; Fukuda, K.; Miyoshi, S.; Konishi, F.; Kodama, H.; Pan, J.; Sano, M.; Takahashi, T.; Hori, S.; Abe, H.; et al. Cardiomyocytes Can Be Generated from Marrow Stromal Cells *in Vitro*. *J. Clin. Invest.* **1999**, *103*, 697–705.
41. Yoon, Y.-S.; Park, J.-S.; Tkebuchava, T.; Luedeman, C.; Losordo, D. W. Unexpected Severe Calcification after Transplantation of Bone Marrow Cells in Acute Myocardial Infarction. *Circulation* **2004**, *109*, 3154–3157.
42. Hwang, S.-T.; Kang, S.-W.; Lee, S.-J.; Lee, T.-H.; Suh, W.; Shim, S. H.; Lee, D.-R.; Taite, L. J.; Kim, K.-S.; Lee, S.-H. The Expansion of Human Es and Ips Cells on Porous Membranes and Proliferating Human Adipose-Derived Feeder Cells. *Biomaterials* **2010**, *31*, 8012–8021.
43. Roell, W.; Lewalter, T.; Sasse, P.; Tallini, Y. N.; Choi, B.-R.; Breitbach, M.; Doran, R.; Becher, U. M.; Hwang, S.-M.; Bostani, T.; et al. Engraftment of Connexin 43-Expressing Cells Prevents Post-Infarct Arrhythmia. *Nature* **2007**, *450*, 819–824.
44. Chen, H.-S. V.; Kim, C.; Mercola, M. Electrophysiological Challenges of Cell-Based Myocardial Repair. *Circulation* **2009**, *120*, 2496–2508.

45. Chang, M. G.; Tung, L.; Sekar, R. B.; Chang, C. Y.; Cysyk, J.; Dong, P.; Marbán, E.; Abraham, M. R. Proarrhythmic Potential of Mesenchymal Stem Cell Transplantation Revealed in an *in Vitro* Coculture Model. *Circulation* **2006**, *113*, 1832–1841.
46. Song, H.; Hwang, H. J.; Chang, W.; Song, B.-W.; Cha, M.-J.; Kim, I.-K.; Lim, S.; Choi, E. J.; Ham, O.; Lee, C. Y.; et al. Cardiomyocytes from Phorbol Myristate Acetate-Activated Mesenchymal Stem Cells Restore Electromechanical Function in Infarcted Rat Hearts. *Proc. Natl. Acad. Sci. U. S. A.* **2011**, *108*, 296–301.
47. Hahn, J.-Y.; Cho, H.-J.; Kang, H.-J.; Kim, T.-S.; Kim, M.-H.; Chung, J.-H.; Bae, J.-W.; Oh, B.-H.; Park, Y.-B.; Kim, H.-S. Pre-Treatment of Mesenchymal Stem Cells with a Combination of Growth Factors Enhances Gap Junction Formation, Cytoprotective Effect on Cardiomyocytes, and Therapeutic Efficacy for Myocardial Infarction. *J. Am. Coll. Cardiol.* **2008**, *51*, 933–943.
48. Murasawa, S.; Kawamoto, A.; Horii, M.; Nakamori, S.; Asahara, T. Niche-Dependent Translineage Commitment of Endothelial Progenitor Cells, Not Cell Fusion in General, into Myocardial Lineage Cells. *Arterioscler., Thromb., Vasc. Biol.* **2005**, *25*, 1388–1394.
49. Plotnikov, E.; Khryapenkova, T.; Vasileva, A.; Marey, M.; Galkina, S.; Isaev, N.; Sheval, E.; Polyakov, V.; Sukhikh, G.; Zorov, D. Cell-to-Cell Cross-Talk between Mesenchymal Stem Cells and Cardiomyocytes in Co-Culture. *J. Cell. Mol. Med.* **2008**, *12*, 1622–1631.
50. Mohanty, S.; Bose, S.; Jain, K. G.; Bhargava, B.; Airan, B. Tgfβ1 Contributes to Cardiomyogenic-Like Differentiation of Human Bone Marrow Mesenchymal Stem Cells. *Int. J. Cardiol.* **2013**, *163*, 93–99.
51. He, X.-q.; Chen, M.-s.; Li, S.-H.; Liu, S.-m.; Zhong, Y.; Kinkaid, H. Y. M.; Lu, W.-Y.; Weisel, R. D.; Li, R.-K. Co-Culture with Cardiomyocytes Enhanced the Myogenic Conversion of Mesenchymal Stromal Cells in a Dose-Dependent Manner. *Mol. Cell. Biochem.* **2010**, *339*, 89–98.
52. Connell, J. P.; Augustini, E.; Moise, K. J.; Johnson, A.; Jacot, J. G. Formation of Functional Gap Junctions in Amniotic Fluid-Derived Stem Cells Induced by Transmembrane Co-Culture with Neonatal Rat Cardiomyocytes. *J. Cell. Mol. Med.* **2013**, *17*, 774–781.
53. Antonitsis, P.; Ioannidou-Papagiannaki, E.; Kaidoglou, A.; Papakonstantinou, C. *In Vitro* Cardiomyogenic Differentiation of Adult Human Bone Marrow Mesenchymal Stem Cells. The Role of 5-Azacytidine. *Interact. Cardiovasc. Thorac. Surg.* **2007**, *6*, 593–597.
54. Hescheler, J.; Meyer, R.; Plant, S.; Krautwurst, D.; Rosenthal, W.; Schultz, G. Morphological, Biochemical, and Electrophysiological Characterization of a Clonal Cell (H9c2) Line from Rat Heart. *Circ. Res.* **1991**, *69*, 1476–1486.
55. Gryshchenko, A. Changes in Expression of the Ion Channels in Mammalian Cardiomyocytes in Early Embryogenesis. *Neurophysiology* **1998**, *30*, 185–189.
56. Yang, L.; Cheng, F.; Liu, T.; Lu, J. R.; Song, K.; Jiang, L.; Wu, S.; Guo, W. Comparison of Mesenchymal Stem Cells Released from Poly(N-Isopropylacrylamide) Copolymer Film and by Trypsinization. *Biomed. Mater.* **2012**, *7*, 035003.
57. Huang, C. C.; Tsai, H. W.; Lee, W. Y.; Lin, W. W.; Chen, D. Y.; Hung, Y. W.; Chen, J. W.; Hwang, S. M.; Chang, Y.; Sung, H. W. A Translational Approach in Using Cell Sheet Fragments of Autologous Bone Marrow-Derived Mesenchymal Stem Cells for Cellular Cardiomyoplasty in a Porcine Model. *Biomaterials* **2013**, *34*, 4582–4591.
58. Shimizu, T.; Yamato, M.; Isoi, Y.; Akutsu, T.; Setomaru, T.; Abe, K.; Kikuchi, A.; Umezu, M.; Okano, T. Fabrication of Pulsatile Cardiac Tissue Grafts Using a Novel 3-Dimensional Cell Sheet Manipulation Technique and Temperature-Responsive Cell Culture Surfaces. *Circ. Res.* **2002**, *90*, E40–E48.
59. Ku, S. H.; Ryu, J.; Hong, S. K.; Lee, H.; Park, C. B. General Functionalization Route for Cell Adhesion on Non-Wetting Surfaces. *Biomaterials* **2010**, *31*, 2535–41.
60. Manickam, S. S.; Gelb, J.; McCutcheon, J. R. Pore Structure Characterization of Asymmetric Membranes: Non-Destructive Characterization of Porosity and Tortuosity. *J. Membr. Sci.* **2014**, *454*, 549–554.
61. Sirc, J.; Hobzova, R.; Kostina, N.; Munzarova, M.; Juklickova, M.; Lhotka, M.; Kubinova, S.; Zajicova, A.; Michalek, J. Morphological Characterization of Nanofibers: Methods and Application in Practice. *J. Nanomater.* **2012**, *2012*, 1.